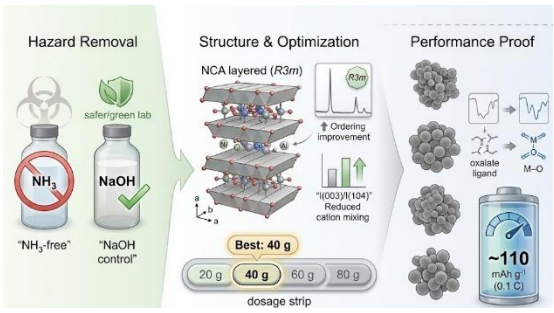
***JKPK (JURNAL KIMIA DAN PENDIDIKAN KIMIA)**, Vol. 10, No. 3, 2025* *pp. 595-609*
Chemistry Education Study Program, Universitas Sebelas Maret *ISSN 2503-4146*
https://jurnal.uns.ac.id/jkpk *ISSN 2503-4154 (online)*

Safer and Sustainable Co-precipitation Synthesis of NCA ($LiNi_{0.80}Co_{0.15}Al_{0.05}O_2$) Cathodes: Eliminating Ammonia in Favor of NaOH for pH Control

Shofirul Sholikhatun Nisa[1*], Meidiana Arinawati[2], Cornelius Satria Yudha[2], Anisa Raditya Nurohmah[3]

[1]Department of Chemical Engineering, Faculty of Industrial Engineering, Universitas Pembangunan Nasional Veteran Yogyakarta, Sleman, Indonesia
[2]Centre of Excellence for Electrical Energy Storage Technology, Universitas Sebelas Maret, Surakarta, Indonesia
[3]Department of Materials Engineering and Convergence Technology, Gyeongsang National University, Jinju, South Korea

ABSTRACT



Developing safer and more sustainable synthesis routes for lithium-ion battery cathodes is important for both environmental practices and laboratory education. This study reports an ammonia-free oxalate coprecipitation route for synthesizing LiNi0.80Co0.15Al0.05O2 (NCA), in which ammonia, typically used as a pH controller, is fully replaced by sodium hydroxide (NaOH). NaOH dosage was varied at 20 g, 40 g, 60 g, and 80 g to control precipitation, precursor quality, and the properties of the final cathode after calcination and sintering. X-ray diffraction confirmed the formation of a layered α NaFeO2-type structure with R3m symmetry for all samples without detectable secondary phases. The 40 g NaOH condition showed the best structural ordering, reflected by a relatively high I(003)/I(104) intensity ratio associated with reduced cation mixing. Fourier transform infrared spectra verified the decomposition of the oxalate ligand during thermal treatment and the appearance of metal-oxygen lattice vibrations consistent with NCA formation. Scanning electron microscopy revealed that the 40 g NaOH sample produced more uniform particles with a narrower size distribution than other variants. Based on these results, the 40 g NaOH sample was selected for electrochemical evaluation and delivered an initial discharge capacity of about 110 mAh g^{-1} at 0.1 C in a full cell configuration. Overall, NaOH is demonstrated as an effective and safer substitute for ammonia in oxalate coprecipitation, enabling greener NCA synthesis protocols for research and teaching.

Keywords: *Ammonia-free; Li-ion battery; NCA; NaOH; safer synthesis*
**Corresponding Author:* *shofirulsholikhatun.nisa@upnyk.ac.id*
How to cite: S.S. Nisa, M. Arinawati, C.S. Yudha, and A. R. Nurohmah, "Safer and Sustainable Co-precipitation Synthesis of NCA ($LiNi_{0.80}Co_{0.15}Al_{0.05}O_2$) Cathodes: Eliminating Ammonia in Favor of NaOH for pH Control," *Jurnal Kimia dan Pendidikan Kimia (JKPK)*, vol. 10, no. 3, pp.595-609, 2025. [Online]. Available: https://doi.org/10.20961/jkpk.v10i3.108184
Received: *2025-08-18* ***Accepted:*** *2025-12-12* ***Published:*** *2025-12-31*

INTRODUCTION

Lithium-ion batteries (LIBs) are among the most widely used energy storage technologies today, particularly in electric vehicles and portable electronic devices [1]. LIBs are rechargeable electrochemical systems that operate through the reversible insertion and extraction of lithium ions (intercalation and deintercalation) between the cathode and anode during charge and discharge cycles. During charging, lithium ions migrate from the cathode to the anode through the electrolyte, while electrons travel through the external circuit. During discharge,

©2025 The Authors. This open-access article is distributed under a (CC-BY-SA License)

the process reverses, allowing for the efficient delivery of electrical energy [2][3].

A typical LIB consists of four main components: (i) a cathode, commonly a lithium transition metal oxide such as $LiNi_{1-x-y}Co_xAl_yO_2$ (NCA), $LiNi_{1-x-y}Mn_xCo_yO_2$ (NMC), or $LiFePO_4$ (LFP); (ii) an anode, most often graphite; (iii) an electrolyte containing a lithium salt dissolved in organic solvents; and (iv) a separator that prevents short circuits while allowing lithium ion transport [3]. Among these components, the cathode has a significant influence on battery capacity, operating voltage, and cycle life, making it a key determinant of overall performance. Various cathode chemistries have been developed, including layered $LiCoO_2$, spinel $LiMn_2O_4$, olivine-type LFP, and nickel-rich layered oxides such as NCA and NMC [4].

Nickel-based layered oxides are particularly attractive due to their high specific capacity and low cost compared to cobalt-rich compositions. However, nickel-rich cathodes suffer from structural instability, cation mixing (Ni^{2+}/Li^{+} disorder), and poor thermal stability, which can compromise both safety and long-term performance [5][6][7]. To address these limitations, small amounts of cobalt and aluminum are commonly incorporated. Cobalt improves structural ordering and electronic conductivity, while aluminum enhances thermal stability and suppresses undesirable phase transitions during cycling [4][7]. As a result, NCA has become a leading candidate for electric vehicle (EV) applications, offering high energy density while maintaining sufficient stability under operating conditions. The performance of NCA strongly depends on its synthesis method, which determines phase purity, particle size, morphology, and cation distribution. Various synthesis routes have been explored, including sol–gel, hydrothermal, spray pyrolysis, solid-state reaction, and co-precipitation. While sol–gel and hydrothermal methods can provide good compositional control, they are often time-consuming, energy-intensive, or difficult to scale up. Spray pyrolysis, although capable of producing fine powders, requires sophisticated equipment and high operational costs. In contrast, co-precipitation is considered the most economically feasible and scalable method for producing homogeneous precursors with controlled particle size and morphology, making it a widely adopted method for commercial cathode production [8].

Co-precipitation processes can be broadly grouped into three routes based on the precipitating agent employed. The basic route, which utilizes hydroxide precipitation, often yields spherical secondary particles with good tap density; however, it is highly sensitive to operating conditions and can lead to compositional inhomogeneity. The neutral route, commonly based on carbonate precipitation, generally provides more stable conditions; however, it frequently yields precursors with irregular particle morphology that may adversely affect electrochemical performance. The acid route, particularly oxalate precipitation, offers specific advantages for cobalt-containing systems. Oxalic acid can stabilize Co2+ ions in solution, promoting uniform nucleation and producing precursors with improved homogeneity and morphology. The oxalate

route also enables better control of particle size and size distribution, making it an attractive approach for synthesizing layered oxide cathode materials [9][10].

Despite these advantages, using oxalic acid alone has several limitations. As a strong organic acid, it is corrosive and may generate acidic byproducts, such as H2SO4, when sulfate salts are used as precursors, which can reduce yield and complicate process control. To address these issues, ammonia has often been used as a pH buffer during oxalate co-precipitation [11]. Ammonia helps maintain stable precipitation conditions and can improve particle uniformity and morphology. However, ammonia poses safety and environmental concerns because it is toxic and volatile, creating health risks in laboratory and industrial environments [12]. In addition, most ammonia is produced from natural gas through the Haber-Bosch process, which is energy-intensive and associated with substantial carbon emissions, making ammonia less compatible with green chemistry principles [13].

Sodium hydroxide (NaOH) has been proposed as an alternative pH controller in oxalate co-precipitation to address the limitations associated with ammonia. NaOH is nonvolatile, easier to handle, and generally presents fewer safety concerns than ammonia. Previous work has shown that NaOH-assisted oxalate co-precipitation can produce NCA precursors under controlled conditions, typically in the pH range of 3 to 4 [14]. However, the effect of NaOH dosage on precursor formation and on the resulting NCA cathode properties has not been systematically examined. In particular, the relationships between NaOH amount, phase formation, particle morphology, and electrochemical performance remain insufficiently understood. Developing ammonia-free synthesis routes for NCA is therefore an important objective for greener and safer cathode manufacturing.

This study presents an ammonia-free oxalate co-precipitation method for synthesizing NCA precursors, utilizing NaOH as a safer and more environmentally benign pH controller. Structural, chemical, and morphological characterizations were conducted to determine the optimal synthesis condition, followed by electrochemical testing of the most promising sample to evaluate its battery performance. The findings contribute to the development of a more sustainable NCA synthesis strategy and provide practical insight for applications where safety and environmental considerations are critical.

METHODS

1. Materials

This study used Nickel sulfate hexahydrate ($NiSO_4.6H_2O$, Zenith Chemical Corporation), cobalt sulfate heptahydrate ($CoSO_4.7H_2O$), Schmudt Chemie Gmbh), aluminium sulfate octadecahydrate ($Al_2(SO_4)_3.18H_2O$, Mahkota), lithium hydroxide monohydrate ($LiOH.H_2O$, Leverton), oxalic acid dihydrate ($H_2C_2O_2.2H_2O$, YC Chemicals Ltd), and sodium hydroxide (NaOH, Asahi) were used as raw materials. All chemicals were of technical grade and used without further purification. Deionized water was used in all preparation steps.

The materials used for electrode preparation and cylindrical cell fabrication,

including acetylene black (AB), carboxymethyl cellulose (CMC), styrene–butadiene rubber (SBR), graphite, polypropylene (PP) separator, and $LiPF_6$ electrolyte. All materials were battery-grade and supplied by Shandong Gelon Lib Co., Ltd.

2. Synthesis Procedures

A mixed solution of Ni, Co, and Al was prepared with a mole ratio of Ni:Co: Al = 0.80:0.15:0.05 and adjusted to a final concentration of 1 M. Separately, 1 M oxalic acid solution was prepared as the chelating agent, while NaOH was used as the pH-controlling agent, with mass variations of 20 g, 40 g, 60 g, and 80 g dissolved in 250 mL of distilled water.

The mixed Ni–Co–Al solution was slowly added dropwise into the oxalic acid solution under continuous stirring at 600 rpm. Subsequently, NaOH solution was added dropwise. The reaction mixture was maintained at 60 °C for 4 hours under constant stirring at 600 rpm to allow for the complete precipitation of the NCA precursor, followed by a 2-hour aging process. The resulting precipitate was filtered and thoroughly washed with deionized water until the filtrate reached neutral pH, then dried in an oven at 100 °C overnight. The dried NCA precursor powder was mixed with lithium hydroxide monohydrate at a molar ratio of 1:1.05 (precursor: $LiOH{\cdot}H_2O$) to compensate for lithium loss during calcination. The precursor–LiOH mixture was first calcined at 500 °C for five hours to remove volatile components, followed by sintering at 800 °C for 12 hours to form the layered NCA cathode structure. Both processes were carried out in an oxygen atmosphere. The obtained NCA powder was sieved through a 200-mesh screen to ensure uniform particle size distribution before characterization and charge-discharge testing. The samples were named based on the mass of NaOH used, with precursor labeled PNCA-NaOH 20, PNCA-NaOH 40, PNCA-NaOH 60, and PNCA-NaOH 80, corresponding to 20 g, 40 g, 60 g, and 80 g of NaOH, respectively. The same nomenclature is maintained for the final cathode materials.

3. Material Characterization

The phase composition and crystallographic structure of the synthesized NCA powders were analyzed using X-ray diffraction (XRD, EQ-MD-10-LD Precision Mini XRD, MTI) with Cu Kα radiation λ = 1.5406 Å at a 2θ range of 15–70° and a scan speed of 0.2 $degree^{-1}$. The diffraction patterns were collected to identify the formation of layered NCA and to determine phase purity. The chemical bonding and functional groups of the precursor and calcined NCA were investigated using Fourier-transform infrared spectroscopy (FTIR, Shimadzu FTIR Spectrometer) in ATR mode over the range of 400–4000 cm^{-1}. The morphology and particle size distribution of the synthesized NCA powders were observed using scanning electron microscopy (SEM, JCM 7000, JEOL) with an accelerating voltage of 15 kV, a working distance of 14.3 mm, and without the use of a conductive coating. SEM imaging was used to examine particle shape, surface texture, and agglomeration behavior.

4. Electrochemical Testing

Charge–discharge testing was conducted on the best-performing NaOH variant, based on previous characterization results showing the most favorable lattice characteristics, well-defined functional groups, and a uniform particle morphology. The NCA cathode material was prepared into a slurry by mixing NCA powder, AB, CMC, SBR, and oxalic acid in a mass ratio of 89:6:3:1:1, respectively. Deionized water was then added to the mixture with a weight ratio of 1:1. The resulting slurry was uniformly coated onto one side of an aluminum foil current collector, with a coating thickness of approximately 200 μm, and subsequently dried in an oven at 80°C until it was fully dry. The same process was repeated on the opposite side of the foil to produce a double-sided cathode sheet. The prepared cathode sheets were then assembled into 18650 cylindrical cells (18 mm diameter and 65 mm height) in a dry room, using graphite sheets as the anode and a polypropylene separator. The electrolyte used was 1 M $LiPF_6$ (EC: EMC = 3: 7), and the electrolyte filling was performed inside an argon-filled glovebox. The fabricated 18650 cells were subjected to galvanostatic charge–discharge testing using a Neware Battery Analyzer with BTS software to record the electrochemical response, within a voltage range of 2.5–4.3 V at a rate of 0.1 C. The raw data obtained from the analyzer were subsequently processed and analyzed using Origin software.

RESULT AND DISCUSSION

The synthesis of $LiNi_{0.80}Co_{0.15}Al_{0.05}O_2$ (NCA) cathode material via ammonia-free oxalate co-precipitation was investigated to understand the influence of NaOH on the structural, chemical, and morphological properties of the resulting powders. The formation of the NCA cathode material proceeded via two main steps: precursor precipitation and subsequent calcination and sintering. Aqueous solutions of transition metal salts (Ni, Co, Al) were co-precipitated using oxalic acid dihydrate in the presence of NaOH. In this step, precursor of Ni, Co, and Al was obtained, while sodium sulfate remained in the aqueous phase as a by-product. The dried precursor was subsequently mixed with lithium hydroxide monohydrate and calcined in an oxygen atmosphere. During calcination, the oxalate and hydroxide species decomposed, releasing CO_2 and H_2O, and the layered oxide phase was formed. The simplified reaction can be expressed as follows:

Precursor formation:

$$0.8NiSO_4 + 0.15CoSO_4 + 0.0.25Al_2(SO_4)_3 + 0.95H_2C_2O_4 + 2.05NaOH \rightarrow 0.8NiC_2O_4.2H_2O + 0.15CoC_2O_4.2H_2O + 0.05Al(OH)_3 + 1.025\,Na_2SO_4 \quad (1)$$

Product formation:

$$0.8NiC_2O_4.2H_2O + 0.15CoC_2O_4.2H_2O + 0.05Al(OH)_3 + LiOH.H_2O + 0.9625O_2 \rightarrow LiNi_{0.80}Co_{0.05}Al_{0.05}O_2 + 1.9CO_2 + 2.975H_2O \quad (2)$$

1. XRD Analysis

To further elucidate the impact of NaOH on the formation of NCA cathodes, the structure of the synthesized powders was first examined by XRD. XRD patterns of the NCA precursors are shown in Figure 1. The XRD patterns of all NCA precursors are similar to nickel oxalate dihydrate ($NiC_2O_4.H_2O$), typically indexed to the JCPDS cards No. 25-0581 [15][16]. Characteristic diffraction peaks appear at 2θ corresponding to the (202), (004), (400), and (022) reflections, confirming successful formation of the intended oxalate precursor [14]. No extraneous peaks from impurities were detected, indicating phase purity across all samples.

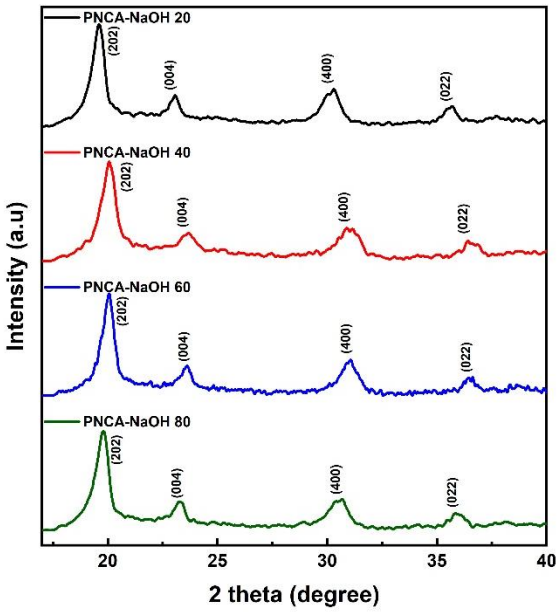


Figure 1. XRD pattern of NCA precursor with varying amounts of NaOH

Table 1. Orthorhombic lattice parameters (a, b, c) and unit cell volume (V) of the NCA precursors

Sample	a (Å)	b (Å)	c (Å)	Volume (Å^3)
PNCA-NaOH 20	11.809	5.014	15.401	911.958
PNCA-NaOH 40	11.560	5.226	15.010	906.858
PNCA-NaOH 60	11.520	5.211	15.086	905.555
PNCA-NaOH 80	11.637	5.307	15.239	941.059

The orthorhombic lattice parameters of the NCA oxalate precursors are shown in Table 1. All samples exhibit a smaller lattice parameter than nickel oxalate dihydrate (a = 11.762 Å, b = 5.332 Å, c = 15.726 Å) [17], with the slight differences attributed to the incorporation of Co and Al atoms into the crystal lattice [14].

Figure 2 compares the XRD patterns of NCA synthesized using different NaOH amounts with a commercial NCA reference. All diffractograms show the set of reflections typical of a layered α NaFeO2 type structure with rhombohedral symmetry (space group R3m), consistent with the standard NCA pattern (JCPDS No. 87 1562) [14][15]. The presence of the low-angle (003) reflection, together with the clear (101), (104), (006)/(102), (108)/(110), and (113) peaks, confirms the formation of a well-developed layered oxide framework. Peak splitting in the (006)/(102) and (108)/(110) regions is also

evident, which is commonly regarded as a signature of good layered ordering in Ni-rich cathode materials. In addition, variations in peak sharpness and relative intensity among the synthesized samples indicate that NaOH dosage influences crystallinity and cation ordering, even though the overall phase remains the same. Importantly, no additional reflections attributable to impurity phases were observed within the measured range, suggesting that the oxalate co-precipitation route produced phase-pure NCA across all NaOH conditions.

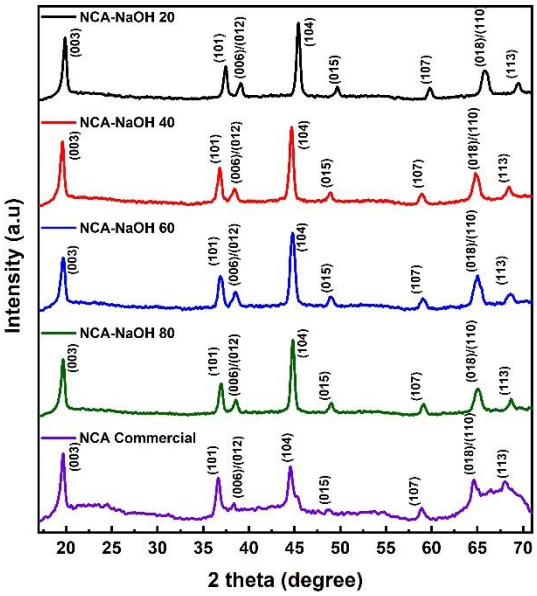


Figure 2. XRD pattern of NCA cathode material

Table 2. Lattice parameter of the NCA cathode material

Sample	a (Å)	c (Å)	c/a	$\frac{I(003)}{I(104)}$
NCA-NaOH 20	2.811	13.868	4.933	0.786
NCA-NaOH 40	2.862	14.017	4.897	0.832
NCA-NaOH 60	2.862	13.921	4.864	0.680
NCA-NaOH 80	2.851	13.989	4.907	0.728
NCA Commercial	2.872	14.066	4.880	1.258

Table 2 shows that the lattice constants a and c decrease at lower NaOH dosages. The NCA NaOH 20 sample exhibits the smallest a and c values, indicating a more compact lattice. In contrast, the commercial NCA sample shows the largest lattice constants, suggesting a comparatively more expanded crystal structure.

Among the synthesized materials, NCA NaOH 40 exhibits the most favorable structural ordering. Its 'a and' c 'values are closest to those of the commercial NCA, and its' c/a' ratio indicates a well-developed layered structure. In addition, the I(003)/I(104) intensity ratio, which is commonly used to evaluate crystallinity and the extent of Li Ni cation mixing, is relatively high for NCA NaOH 40. This result suggests reduced cation disorder and improved layered ordering compared with the other synthesized samples. Previous studies have consistently reported that c/a ratios close to

or above 4.9, along with high I(003)/I(104) values, are characteristic of well-ordered R3m layered cathodes with minimized cation mixing, which is beneficial for electrochemical performance.[18][19].

2. FTIR Analysis

FTIR spectroscopy was conducted to complement the structural analysis by tracking the evolution of chemical bonds during precursor decomposition. This technique provides evidence for the removal of oxalate ligands and the formation of metal-oxygen (M–O) bonds, thereby supporting the effectiveness of the calcination and sintering steps.

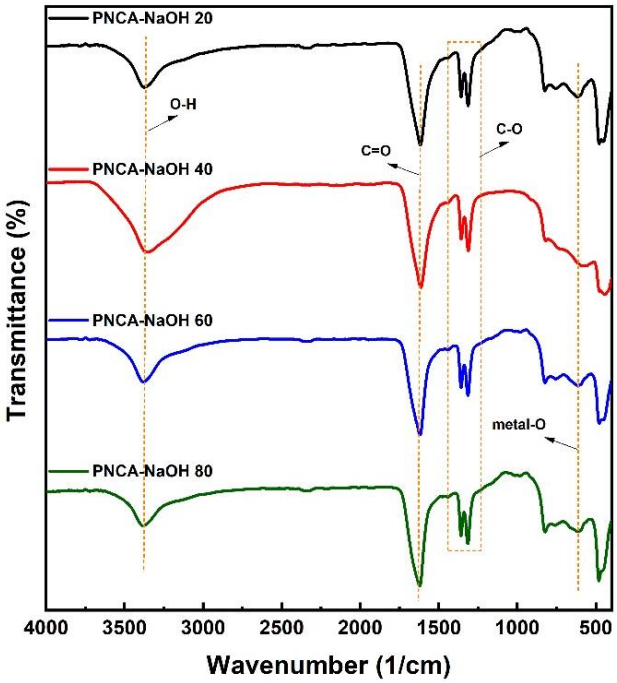


Figure 3. FTIR spectra of NCA precursor with varying amounts of NaOH

Figure 3 shows the FTIR spectra of the synthesized NCA precursors. The spectra display absorption features characteristic of hydrated metal oxalate species. Broad bands in the 3360 to 3380 cm^{-1} region are assigned to O–H stretching vibrations from interlayer and surface adsorbed water, which are commonly observed in metal oxalate hydrates. Strong bands in the 1315 to 1620 cm^{-1} range correspond to the asymmetric and symmetric stretching vibrations of coordinated oxalate groups ($C_2O_4^{2-}$), confirming that oxalate ligands are incorporated into the precursor structure. Additional bands near 600 cm^{-1} are attributed to metal oxygen stretching vibrations, indicating the presence of a mixed metal oxalate framework[20].

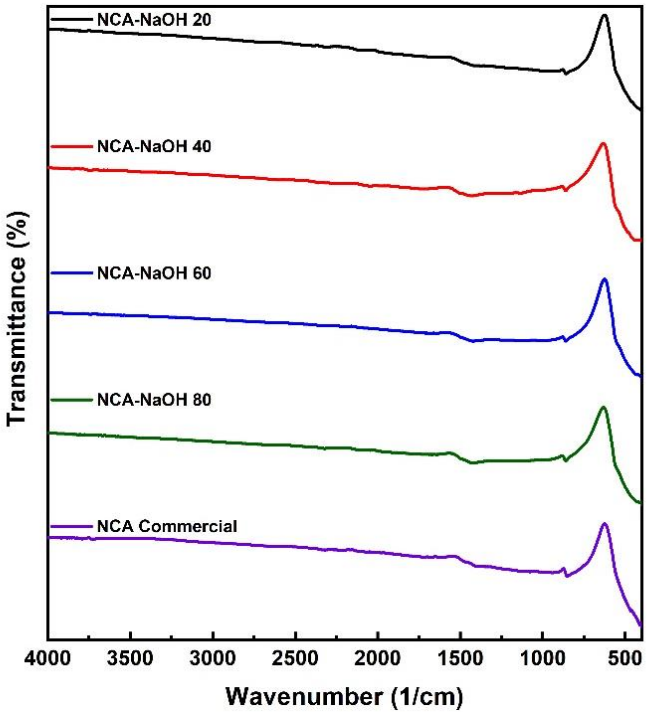


Figure 4. FTIR spectra of NCA cathode material

Figure 4 shows the FTIR spectra of calcined NCA cathodes, which reveal the successful transformation of the oxalate precursors into the layered oxide phase. Characteristic absorption bands associated with oxalate groups (C=O and C–O at 1620 cm^{-1} and 1315 cm^{-1}) and intercalated water (O–H stretching at 3360-3380 cm^{-1}) are no longer observed, confirming the complete decomposition of the oxalate precursor during calcination. This is consistent with the formation of the expected α-$NaFeO_2$-type layered structure of NCA. Intense absorptions dominate the spectra of all samples at around 600 cm^{-1}, which correspond to M–O (Ni–O, Co–O, Al–O) stretching vibrations in the layered NCA lattice.[21][22]. The FTIR spectra of the synthesized samples are comparable to those of the commercial NCA material, further validating the effectiveness of this synthesis route. Overall, the variation in NaOH concentration did not lead to significant differences in chemical bonding or functional group composition.

3. SEM Analysis

Beyond structural and chemical characterization, SEM was used to examine the morphology and particle size distribution of the synthesized NCA powders. The SEM results indicate that the NaOH dosage plays a crucial role in controlling particle shape, size uniformity, and agglomeration behavior.

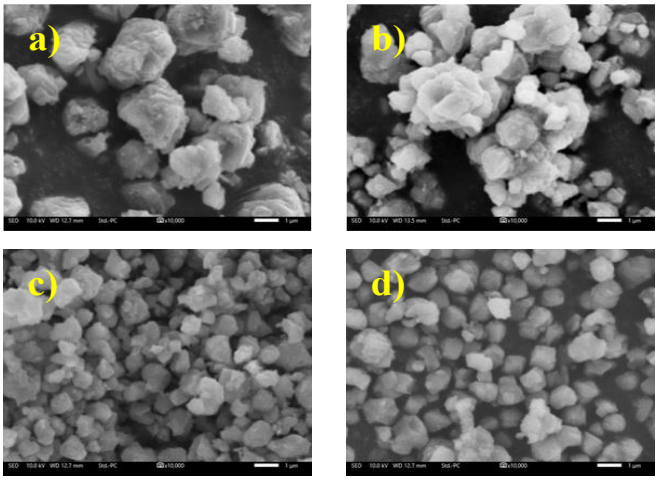


Figure 5. SEM image at 10,000x magnification of NCA precursor with varying amounts of NaOH: a) 20 g, b) 40 g, c) 60 g, and d) 80 g.

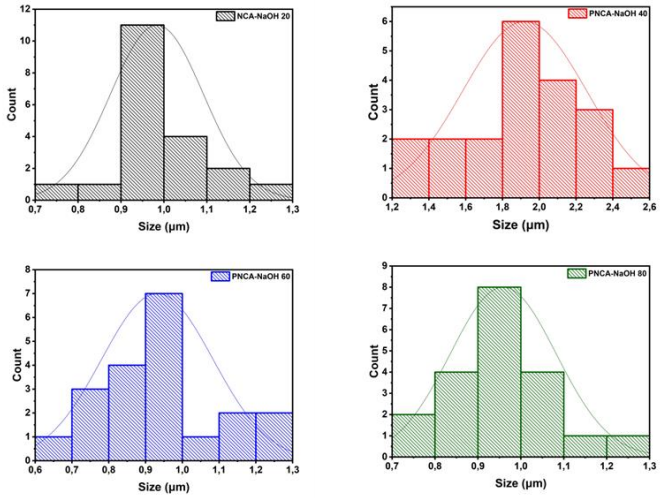


Figure 6. Particle size histogram of NCA precursor with varying amounts of NaOH

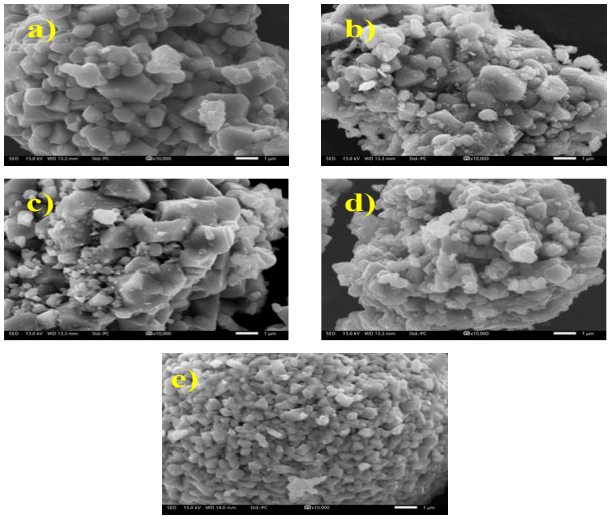


Figure 7. SEM image at 10,000x magnification of NCA cathode material: a) NaOH 20 g, b) NaOH 40 g, c) NaOH 60 g, d) NaOH 80 g, and e) commercial

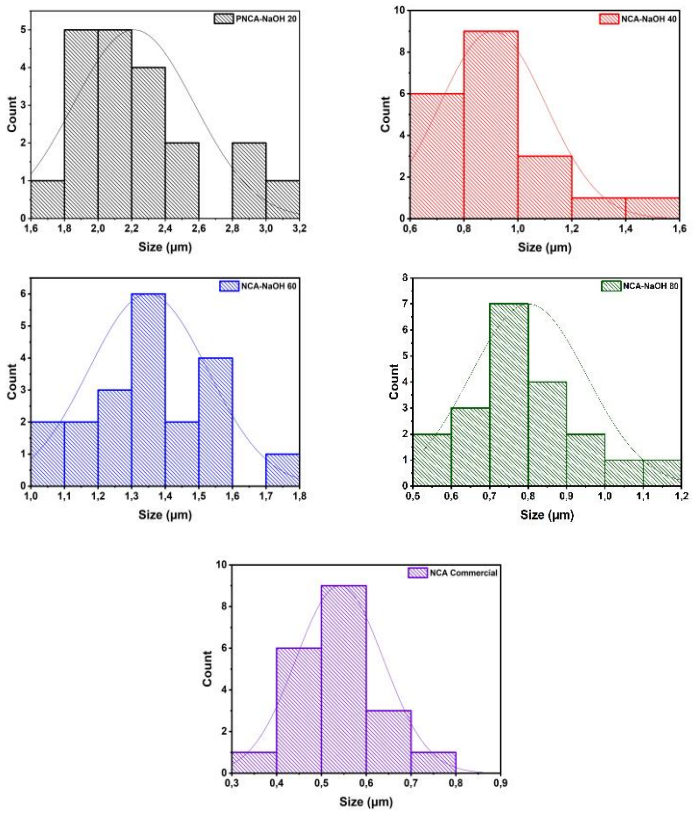


Figure 8. Particle size histogram of NCA cathode material

At the lowest NaOH dosage (Figure 5a), the precursor particles exhibit irregular morphology and strong agglomeration, forming dense clusters with a broad size distribution of approximately 1.6–3.2 μm (Figure 6). Increasing the NaOH amount to 40 g (Figure 5b) yields particles that remain relatively large (approximately 1.2–2.6 μm), yet the particle boundaries become more clearly defined, and the surface appears rougher. A more pronounced improvement is observed at higher NaOH dosages. Precursors prepared with 60 g and 80 g NaOH (Figures 5c and 5d) show better particle uniformity and a narrower size distribution, with particles that are more rounded, discrete, and more homogeneously dispersed.

Morphological evolution after calcination and sintering is shown in Figure 7, while the corresponding particle size distributions are presented in Figure 8. Compared with the precursor stage, the final NCA powders exhibit notable microstructural changes. NCA NaOH 20 shows agglomerated particles with clearer interparticle boundaries. NCA NaOH 40 displays improved necking and grain bonding while still retaining distinguishable grain boundaries. A major change occurs for NCA NaOH 60, where the particles become highly fused and irregular, resulting in large agglomerates. This suggests that although the 60 g NaOH precursor initially exhibited a favorable morphology, it likely underwent excessive grain growth during thermal treatment, resulting in undesirable

microstructural features. NCA NaOH 80 shows more uniform grain fusion and slightly more regular particle shapes than the 60 g sample, indicating a more controlled sintering response despite the finer precursor particles. These trends are consistent with the particle size histograms in Figure 8. After sintering, NCA NaOH 60 shifts from a sharp and narrow distribution centered at about 0.9 μm in the precursor stage to a broader distribution, confirming significant particle growth and aggregation. In contrast, NCA NaOH 80 maintains a similar size range before and after sintering, indicating better control over grain growth. NCA NaOH 20 and 40 show moderate reductions in particle size after sintering. In comparison to these samples, the commercial NCA exhibits dominant particle sizes of around 0.5 μm, as shown in Figure 8.

4. Electrochemical Performance

Among the prepared samples, NCA-NaOH 40 was selected for charge-discharge testing based on its consistently exhibiting the best overall combination of structural ordering (the highest I(003)/I(104) ratio among the synthesized samples), complete decomposition of oxalate ligands, and uniform particle morphology with narrow size distribution. During the charging process, Li^+ ions migrate from the cathode through the electrolyte toward the anode, accompanied by electron transfer via the external circuit (Eqs. 3–5). This mechanism is analogous to electrolysis, where electrical energy is stored as chemical potential. In contrast, during discharging, Li^+ ions return from the lithiated anode to the cathode while releasing electrons, resembling the operation of a galvanic cell (Eqs. 6–8). The overall reaction for a complete charge–discharge cycle is summarized in Eq. (9)[7].

Charging:

$LiNi_{0.80}Co_{0.15}Al_{0.05}O_2 \rightarrow xLi^+ + Li_{1-x}Ni_{0.80}Co_{0.15}Al_{0.05}O_2 + xe^-$ (3)

$xLi^+ + xe^- + 6C \rightarrow Li_xC_6$ (4)

$LiNi_{0.80}Co_{0.15}Al_{0.05}O_2 + 6C \rightarrow Li_{1-x}Ni_{0.80}Co_{0.15}Al_{0.05}O_2 + Li_xC_6$ (5)

Discharging:

$xLi^+ + Li_{1-x}Ni_{0.80}Co_{0.15}Al_{0.05}O_2 + xe^- \rightarrow LiNi_{0.80}Co_{0.15}Al_{0.05}O_2$ (6)

$Li_xC_6 \rightarrow xLi^+ + xe^- + 6C$ (7)

$Li_{1-x}Ni_{0.80}Co_{0.15}Al_{0.05}O_2 + Li_xC_6 \rightarrow LiNi_{0.80}Co_{0.15}Al_{0.05}O_2 + 6C$ (8)

Overall reaction:

$LiNi_{0.80}Co_{0.15}Al_{0.05}O_2 + 6C \rightleftarrows Li_{1-x}Ni_{0.80}Co_{0.15}Al_{0.05}O_2 + Li_xC_6$ (9)

The charge-discharge profile in Figure 9 shows a clear voltage plateau at approximately 3.6–3.8 V, characteristic of layered NCA cathodes undergoing reversible lithium intercalation and deintercalation. The initial specific discharge capacity reaches 110.697 mAh g−1 at 0.1 C, indicating good electrochemical activity of the synthesized material. This value remains below the theoretical capacity of about 180 mAh g−1, which is expected because the evaluation was conducted in a full cell configuration using a graphite anode rather than lithium metal, and the full cell capacity is limited by

electrode balancing and practical cell polarization.

A combined interpretation of the XRD, FTIR, SEM, and electrochemical results clarifies how structural and morphological features influence lithium storage performance. XRD indicates that the 40 g NaOH sample exhibits the highest structural ordering, as reflected by an elevated I(003)/I(104) ratio, which is associated with reduced cation mixing and improved layered crystallinity, thereby facilitating lithium ion transport. FTIR confirms the decomposition of the oxalate ligand during thermal treatment, supporting the formation of a stable oxide framework. SEM observations reveal a relatively uniform particle morphology with a narrower size distribution, which can reduce diffusion limitations and enhance electrode-electrolyte contact. These advantages are consistent with the electrochemical performance, where NCA NaOH 40 delivers 110.697 mAh g−1, corresponding to roughly 60% of the theoretical capacity.

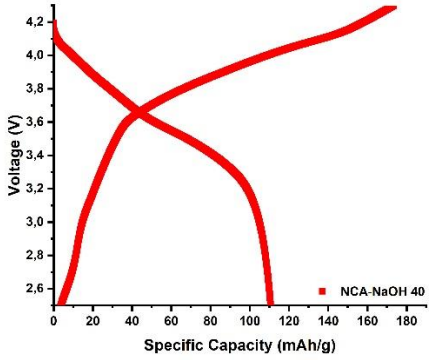


Figure 9. Charge-discharge curve of NCA-NaOH 40

Several limitations should be noted. The NaOH dosages investigated were limited, which may exclude conditions that could further optimize phase formation and microstructure. Additionally, electrochemical testing was conducted on a limited number of samples, thereby reducing the statistical strength. Future work should explore a wider parameter space for synthesis and include more replicate cells to improve the reliability and generalizability of the observed structure-performance relationships.

CONCLUSION

This study demonstrates that the NaOH dosage, particularly 40 g, is crucial for optimizing NCA cathode materials synthesized via oxalate co-precipitation. Overall results confirm that NaOH strongly controls precursor quality and final cathode properties, with 40 g providing the most favorable balance between structural ordering and particle morphology.

XRD indicates that NCA NaOH 40 has a relatively high I(003)/I(104) ratio, implying reduced cation mixing and better layered ordering. FTIR confirms complete oxalate decomposition after calcination and the formation of metal oxygen lattice vibrations in all samples, while NCA NaOH 40 exhibits sharper, more well-defined peaks,

indicating higher crystallinity. SEM reveals that NCA NaOH 40 yields the most uniform morphology, characterized by a relatively narrow particle size distribution (8–12 μm), which supports improved packing and lithium ion transport. Consistent with these features, charge-discharge testing demonstrates reversible lithium insertion and extraction, with an initial discharge capacity of 110.697 mAh g−1 at 0.1 C, or approximately 60% of the theoretical NCA capacity (180–200 mAh g^{-1}). The findings emphasize that controlling the NaOH concentration is essential for regulating precipitation kinetics and nucleation growth behavior in ammonia-free NCA synthesis. Further work should extend the NaOH range with finer increments, evaluate cycling stability and rate capability at multiple C rates, clarify NaOH's mechanistic role using in situ methods, and validate scalability at the pilot scale.

ACKNOWLEDGEMENT

The author would like to express sincere gratitude to Prof. Dr. Eng. Ir. Agus Purwanto, S.T., M.T., as the Head of the Centre of Excellence for Electrical Energy Storage Technology (CE-FEEST), for providing the facilities and support during the implementation of this research. His guidance, encouragement, and valuable insights have greatly contributed to the completion of this work. The author also extends appreciation to all members of CE-FEEST for their kind assistance and cooperation throughout the research activities.

REFERENCES

[1] D. A. Elalfy, E. Gouda, M. F. Kotb, V. Bureš, and B. E. Sedhom, "Comprehensive review of energy storage systems technologies, objectives, challenges, and future trends," *Energy Strateg. Rev.*, vol. 54, no. June, 2024, doi: 10.1016/j.esr.2024.101482.

[2] T. A. Manfo and M. E. Şahin, "Intercalation reaction in lithium-ion battery: effect on cell characteristics," *Int. J. Mater. Eng. Technol.*, vol. 6, no. 2, pp. 70–78, 2023, [Online]. Available: http://dergipark.gov.tr/tijmet

[3] S. A. Arote, "Fundamentals and perspectives of lithium-ion batteries," *Lithium-ion Lithium–Sulfur Batter.*, pp. 1-1-1–26, 2022, doi: 10.1088/978-0-7503-4881-2ch1.

[4] A. K. Koech, G. Mwandila, F. Mulolani, and P. Mwaanga, "Lithium-ion battery fundamentals and exploration of cathode materials: A review," *South African J. Chem. Eng.*, vol. 50, no. June, pp. 321–339, 2024, doi: 10.1016/j.sajce.2024.09.008.

[5] B. Cui, Z. Xiao, S. Cui, S. Liu, X. Gao, and G. Li, *Safety Issues and Improvement Measures of Ni-Rich Layered Oxide Cathode Materials for Li-Ion Batteries*, vol. 7, no. 1. Springer Nature Singapore, 2024. doi: 10.1007/s41918-024-00211-2.

[6] B. Fu, M. Moździerz, A. Kulka, and K. Świerczek, "Recent progress in Ni-rich layered oxides and related cathode materials for Li-ion cells," *Int. J. Miner. Metall. Mater.*, vol. 31, no. 11, pp. 2345–2367, 2024, doi: 10.1007/s12613-024-2948-y.

[7] C. S. Yudha, L. M. Hasanah, S. U. Muzayanha, H. Widiyandari, and A. Purwanto, "Synthesis and Characterization of Material LiNi0.8Co0.15Al0.05O2 Using One-Step Co-Precipitation Method for Li-Ion Batteries," *JKPK (Jurnal Kim. dan Pendidik. Kim*, vol. 4, no. 3, p. 134, 2019, doi: 10.20961/jkpk.v4i3.29850.

[8] A. Purwanto, C. S. Yudha, U. Ubaidillah, H. Widiyandari, T. Ogi, and H. Haerudin, "NCA cathode material: Synthesis methods and performance enhancement efforts," *Mater. Res. Express*, vol. 5, no. 12, 2018, doi: 10.1088/2053-1591/aae167.

[9] B. Huang *et al.*, "Layered Cathode Materials: Precursors, Synthesis, Microstructure, Electrochemical Properties, and Battery Performance," *Small*, vol. 18, no. 20, pp. 1–18, 2022, doi: 10.1002/smll.202107697.

[10] S. Mallick *et al.*, "Low-cobalt active cathode materials for high-performance lithium-ion batteries: synthesis and performance enhancement methods," *J. Mater. Chem. A*, vol. 11, no. 8, pp. 3789–3821, 2023, doi: 10.1039/d2ta08251a.

[11] W. Li, S. Lee, and A. Manthiram, "High-Nickel NMA: A Cobalt-Free Alternative to NMC and NCA Cathodes for Lithium-Ion Batteries," *Adv. Mater.*, vol. 32, no. 33, pp. 1–6, 2020, doi: 10.1002/adma.202002718.

[12] D. A. Khudhur, T. A. Tuan Abdullah, and N. Norazahar, "A Review of Safety Issues and Risk Assessment of Industrial Ammonia Refrigeration System," *ACS Chem. Heal. Saf.*, vol. 29, no. 5, pp. 394–404, 2022, doi: 10.1021/acs.chas.2c00041.

[13] S. C. D'Angelo *et al.*, "Planetary Boundaries Analysis of Low-Carbon Ammonia Production Routes," *ACS Sustain. Chem. Eng.*, vol. 9, no. 29, pp. 9740–9749, 2021, doi: 10.1021/acssuschemeng.1c01915.

[14] C. S. Yudha *et al.*, "Production of nickel-rich LiNi0.89Co0.08Al0.03O2cathode material for high capacity NCA/graphite secondary battery fabrication," *Open Eng.*, vol. 12, no. 1, pp. 501–510, 2022, doi: 10.1515/eng-2022-0051.

[15] A. Jumari, C. S. Yudha, M. Nizam, E. R. Dyartanti, Suranto, and A. Purwanto, "An environmentally friendly hydrometallurgy process for the recovery and reuse of metals from spent lithium-ion batteries, using organic acid," *Open Eng.*, vol. 12, no. 1, pp. 485–494, 2022, doi: 10.1515/eng-2022-0050.

[16] Z. Zhu *et al.*, "Multichannel pathway-enriched mesoporous NiO nanocuboids for the highly sensitive and selective detection of 3-hydroxy-2-butanone biomarkers," *J. Mater. Chem. A*, vol. 7, no. 17, pp. 10456–10463, 2019, doi: 10.1039/c9ta01013k.

[17] H. J. Oh *et al.*, "Nickel oxalate dihydrate nanorods attached to reduced graphene oxide sheets as a high-capacity anode for rechargeable lithium batteries," *NPG Asia Mater.*, vol. 8, no. 5, 2016, doi: 10.1038/am.2016.59.

[18] Q. Ma *et al.*, "Induction and Maintenance of Local Structural Durability for High-Energy Nickel-Rich Layered Oxides," *Small Methods*, vol. 6, no. 6, pp. 1–11, 2022, doi: 10.1002/smtd.202200255.

[19] J. Meng *et al.*, "Modulating Crystal and Interfacial Properties by W-Gradient Doping for Highly Stable and Long Life Li-Rich Layered Cathodes," *Adv. Funct. Mater.*, vol. 32, no. 19, pp. 1–11, 2022, doi: 10.1002/adfm.202113013.

[20] S. M. Kim *et al.*, "Cs desorption behavior during hydrothermal treatment of illite with oxalic acid," *Environ. Sci. Pollut. Res.*, vol. 27, no. 28, pp. 35580–35590, 2020, doi: 10.1007/s11356-020-09675-3.

[21] Z. Zhang *et al.*, "Hierarchical Structure Design of ZIF-Derived CoNiFe LDH Nanocages Grown on Ag Nanowires as High-Performance Cathode for Zn-Air Batteries," *Small*, vol. 21, no. 23, pp. 1–11, 2025, doi: 10.1002/smll.202502344.

[22] C. Lv, Z. Li, X. Ren, K. Li, J. Ma, and X. Duan, "Revealing the degradation mechanism of Ni-rich cathode materials after ambient storage and related regeneration method," *J. Mater. Chem. A*, vol. 9, no. 7, pp. 3995–4006, 2021, doi: 10.1039/d0ta10378k